A Framework for Space Safety Analysis: Fragmentation Footprint and Multi-Shell Critical Density

Di Wu
Embry Riddle Aeronautical University, Daytona Beach, FL, United States

ABSTRACT

We introduce a novel framework that combines simplified analytical models with data- and scenario-driven parameter calibration to provide a holistic quantification of space system safety. Central to this framework is a "fragmentation footprint", a concept analogous to a carbon footprint but focused on debris generation. We also propose a refined definition of critical density in a multi-shell orbital context, offering a more accurate measure for collision risk and sustainability evaluation. Space Situational Awareness (SSA) and Space Domain Awareness (SDA) efforts increasingly require clear, quantifiable methods to assess risk in crowded orbits, especially given the surge in satellite deployments and missions. By bridging the gap between simplified theoretical models and high-fidelity simulations, our approach helps analysts and policymakers evaluate long-term implications of orbital activities with greater confidence. The "fragmentation footprint" concept, in particular, provides a unified metric that can inform strategies for debris mitigation, mission design, and policy-making. Ultimately, our framework aims to strengthen SSA/SDA capabilities by delivering more robust tools to anticipate and manage critical scenarios, supporting safer and more sustainable use of Earth's orbital environment.

1. INTRODUCTION

Space safety is a critical component of modern space engineering, extending well beyond individual missions and programs. Kessler's seminal works [3–5] provided the first traceable framework linking space sustainability and safety. With the rapid emergence of megaconstellations and the increasing accessibility of space, this topic warrants renewed attention. Recent efforts have revisited and enhanced the classical source–sink model [1], while substantial progress has also been made in developing advanced numerical tools and scenario analyses [2, 6, 7].

The term space system broadly encompasses all anthropogenic objects in orbit. A common approach to quantifying their dynamics is shelling the Earth's orbital environment, since most operational and non-operational space objects reside in near-circular trajectories. Kessler's original derivation introduced a mathematical formulation that, for the first time, integrated breakup dynamics into a population-level model of the orbital environment. However, this work largely relied on a single-shell formulation—a simplification that is increasingly inadequate given the emergence of multiple megaconstellations operating across distinct orbital shells. A natural question thus arises: how can the single-shell framework be extended to a general multi-shell formulation? Such an extension would enable a more realistic and comprehensive representation of the evolving space environment.

In this paper, we first revisit Kessler's derivation of the critical condition and critical number. Building upon this foundation, we introduce a new definition of the fragmentation footprint and explicitly derive the condition for multi-shell critical numbers. We then present numerical simulations to illustrate the implications of these formulations. Finally, we conclude with a discussion of their broader significance for space sustainability.

2. SPACE SYSTEM SAFETY FRAMEWORK

2.1 Revisit to Kessler's Derivation

Critical Density for a Runaway Environment. Kessler's seminal work series [3–5] illustrate, for the first time, the limit of the operation environment for space system. One of this series most striking contributions is the expression of the critical density corresponding to a runaway environment ${}_{\mathrm{R}}\mathrm{S}_{\mathrm{i}}$, given as Eq. (4) in [4]

$$ {}_{\mathrm{R}}\mathrm{S}_{\mathrm{i}} = 1/\left(\sigma_{\mathrm{f}} \mathrm{V} \mathrm{N}_0 \tau\right). \tag{1} $$

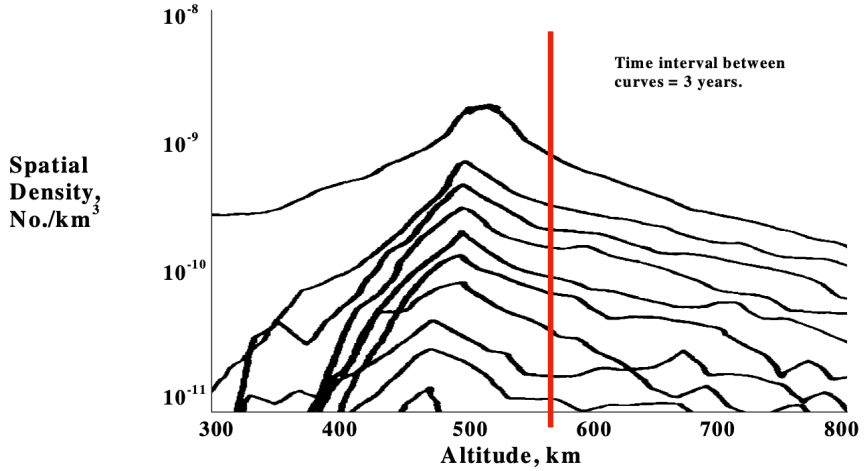

Figure 14. Spatial Density of Modeled Collision Fragments in Kessler, 1991 (Solar Activity = 110, 300 Fragments Generated)

Fig. 1: On Kessler's [4] Figure 14, the time evolution of spatial density is expressed as multiple curves at an interval of 3 years. A time-dependent spatial density at a single height is depicted as a single red line crossing multiple curves at a single height.

This clean result Eq. 1 comes from simply observing the limit condition for the equilibrium solution, given as Eq. (3) in [4] with an extra term for clarification,

$$S_B\,(=S_f) = S_i^2\sigma_i V N_0 \tau/\left(1 - S_i\sigma_f V N_0 \tau\right), \tag{2}$$

where the runaway environment ${}_RS_i$ should satisfy

$$1 - {}_RS_i\sigma_f V N_0 \tau = 0. \tag{3}$$

The Kessler's Dynamics. The equilibrium solution comes from solving Kessler's model between, in his term, "intact spacecraft" and "fragments large enough to catastrophically breakup intact spacecraft" [5], expressed in spatial density as S_i and S_f.

In this environment of S_i and S_f, at any instance, the breakups of intact spacecraft, thus the rate of breakups of intact spacecraft, dB/dt, is expressed as Eq. (2) in [5]

$$dB/dt = S_i^2\sigma_i V\Delta U + S_i\, S_f\sigma_f V\Delta U. \tag{4}$$

Each breakup (in [5] Kessler used the word collision) is assumed to produce a time-dependent spatial density $S_1(t)$ at a single height h_1. Kessler's Figure 14 from [4] is cited here as Fig. 1. The ver

Then the height-dependent spatial density of breakups S_B is, given as Eq. (1) in [5],

$$S_B = dB/dt \int S_1(t)dt. \tag{5}$$

Then, to find the equilibrium solution, we take $S_B = S_f$ and use Eq. 4 and Eq. 5. By taking the following intermediate step,

$$S_f = dB/dt \int S_1(t)dt = S_i^2\sigma_i V\Delta U \int S_1(t)dt + S_i\, S_f\sigma_f V\Delta U \int S_1(t)dt, \tag{6}$$

we arrive at Eq. 7 a solution similar to Eq. 2,

$$S_f = S_i^2\sigma_i V\Delta U \int S_1(t)dt/\left(1 - S_i\sigma_f V\Delta U \int S_1(t)dt\right) \tag{7}$$

The Integral of Spatial Density and Fragments Orbital Lifetime. The difference between Eq. 2 and Eq. 7 is the term $\Delta U \int S_1(t)dt$ and $N_0\tau$. The term $\Delta U \int S_1(t)dt$ is the integral of the time-dependent spatial density at a given height over time and scaled by the volume of consideration. The physical meaning of the term $N_0\tau$ is the time-averaged number of fragments found within the volume over those fragments orbital lifetime [4]. N_0 is the average number of fragments produced per breakup. τ is the characteristic decay time of these fragments and it should satisfy the expression over all objects' lifetime integral,

$$N_0\tau = \int N dt. \tag{8}$$

This term physically describes the accumulation of breakup fragments from the generation moment to their total decay. This matches with the physcial meaning of having integral of spatial density over time and volume $\Delta U \int S_1(t)dt$. Since the integration over time-dependent density $S_1(t)$ produces a height-relevant values, the scaling over the volume is done at the accordingly height. Thus the term $\Delta U \int S_1(t)dt$ is equivalent to having a double integral as used in Eq. (6) and Eq. (7) in [4], thus

$$\Delta U \int S_1(t)dt) = \iint S_1(t)dtdU = N_0\tau. \tag{9}$$

Kessler expressed the time integral for the fragment density using Eq. (10) in [4]. We note this one here with an extra term for clarity.

$$S_t(h)\left(= \int S_1(t)dt\right) = W/(4\pi a^2 da/dt) \tag{10}$$

Employing a circular orbit approximation without losing generality, the rate of change in semi-major axis a is expressed, corresponding to Eq. (11) in [4], as

$$da/dt = a\rho_a C_D V_o A/m. \tag{11}$$

Plugging Eq. 10 and Eq. 11 into Eq. 9, and $dU = 4\pi a^2 dh$, yields

$$N_0\tau = \int S_t(h)dU = \int \frac{W\frac{m}{A}}{(4\pi a^3 \rho_a C_D V_o)} \cdot 4\pi a^2 dh = \int \frac{W\frac{m}{A}}{a\rho_a C_D V_o} dh, \tag{12}$$

Thus,

$$N_0\tau = W\frac{N_0(\frac{m}{A})_{ave}(h_{max} - h_1)}{a_{ave}\rho_a C_D V_o}. \tag{13}$$

With N_0 representing the average number of fragments produced per breakup, the multiplication with the averaged values $\frac{m}{A}_{ave}$ and $a_a ve$ is equivalent to the integration over the whole range, e.g. $\sum_{i=1}^{N_0} \frac{m}{A}_i = N_0(\frac{m}{A})_{ave}$. This range is, according to Kessler's derivation scheme, is set to consider a shelling range of h_1 and h_max. By observing Eq. 13, we could also notice the expression for τ,

$$\tau = W\frac{(\frac{m}{A})_{ave}(h_{max} - h_1)}{a_{ave}\rho_a C_D V_o}. \tag{14}$$

2.2 Definition of Fragmentation Footprint

Critical Number. We have introduced the important concepts of accumulation of breakup fragments from generation to total decay per breakup $N_0\tau$, which strictly should be written as $N_0\tau(h_1, h_max)$ or in general $N_0\tau(h_1, h_2)$, and its expression in Eq. 13; spatial density S_i and critical density for a runway environment ${}_RS_i$ in Eq. 1. The concept of shelling is mentioned in the definition of $N_0\tau$. We approximate the shelling volume ΔU with circular orbit approximation that $a(h)$ being the semimajor axis of the orbits in the shell,

$$\Delta U = \int_{h_1}^{h_2} (4\pi a^2(h)dh) \approx 4\pi a(h_1)^2(h_2 - h_1), \tag{15}$$

As such, we have the shelling-dependent critical number ${}_RN_i$ from spacecraft density ${}_RS_i$ as

$${}_RN_i = {}_RS_i \cdot \Delta U(h_1, h_2), \tag{16}$$

notice the shelling's lower height h_1 needs to be where the orbit decay is considered as a "total decay", which, from a shell perspective, means it is not affecting the generation of breakup B for that shell.

Combining Eq. 1, Eq. 13, Eq. 15 with a replacement of h_{max} for h_2, we reproduce Eq. (7) in [5] as,

$$ {}_{R}N_i = \frac{4\pi a^3(h_1) V_0 \rho_a(h_1) C_D}{\sigma_f V W \left(\frac{m}{A}\right)_{ave} N_0}. \tag{17} $$

Shelling-dependent Critical Potential. ${}_{R}N_i$ is a number of intact objects in the shell between h_1, h_{max} and $N_0\tau$ is the accumulation of breakup fragments from generation to total decay per breakup. Making a reasonable assumption that an intact object can not break up more than once, also proposed in Kessler's assumption as "... capable of catastrophically breaking up an intact object ..." and "a collision between an intact object ... generate N_0 fragments and a collision between two intact objects generates $2N_0$ fragments..." [4], we can arrive at the new variable critical potential ${}_{R}C_i$ as Eq. 18, the "sunk cost" of the critical numbers of intact object.

$$ {}_{R}C_i(h_1, h_{max}) = {}_{R}N_i(h_1) \cdot N_0\tau. \tag{18} $$

The operation yields Eq. 19,

$$ {}_{R}C_i(h_1, h_{max}) = \frac{4\pi a^3(h_1) V_0 \rho_a(h_1) C_D}{\sigma_f V(h_1) W \left(\frac{m}{A}\right)_{ave} N_0} \cdot N_0 W \frac{\left(\frac{m}{A}\right)_{ave}(h_{max} - h_1)}{a_{ave}\rho_a C_D V_o} = \frac{4\pi a^2(h_1)(h_{max} - h_1)}{\sigma_f V}. \tag{19} $$

Shelling-independent Constant Since critical potential is related with the shelling volume ΔU (see Eq. 15), Eq. 19 can be averaged over the volume as

$$ \frac{{}_{R}C_i(h_1, h_{max})}{4\pi a^2(h_1)(h_{max} - h_1)} = \frac{1}{\sigma_f V}. \tag{20} $$

Now we arrive at an expression that is **independent of shelling but only related with the collision nature!** The variable σ_f is the collision area for fragments and V is the "average relative velocity that transforms spatial density into flux and has a value of about 7.5km/sec" [5], in another words, both variables are only related to the collision and breakup nature. Only if the collision nature changes, this constant holds independent of shelling and time at the critical runway scenario.

This constant can also be linked back critical density ${}_{R}S_i$ as

$$ {}_{R}S_i N_0 \tau = \frac{1}{\sigma_f V}. \tag{21} $$

2.3 Multi-Shell Orbital Critical Number Condition

We introduced shelling-dependent critical potential and shelling-independent constant. The potential $C(h_1, h_2)$ could be extended to a general expression as the physical meaning of combining the number of intact objects $N(h_1)$ and $N_0\tau$ the accumulation of breakup fragments from generation to total decay per breakup for every object in the intact objects, thus **Fragmentation Footprint**,

$$ C(h_1, h_2) = N(h_1) \cdot N_0\tau. \tag{22} $$

Formulating in 3 shells So far, we have introduced all the concepts within a single given shell h_1 and h_2/h_{max}. When there are multiple shells coexisting, we can extend the single shell potential formulation. When we consider there are three shells in total, with the height h_1 as the out of system height, h_{S1}, h_{S2}, h_{S3} the three boundaries for the shells. The total potential could be formulated as following: For the critical number of intact objects in region I between h_1 and h_{S1}, the scaling α_1 is used to scale this critical number from single shell derivation to satisfy multiple-shell condition,

$$ \frac{C_I}{4\pi a_{h1}^2(h_{S1} - h_1)} = \frac{1}{4\pi a_{h1}^2(h_{S1} - h_1)} \cdot \alpha_1 \cdot {}_{C}N(h_1, h_{S1}) \cdot N_0\tau(h_1, h_{S1}). \tag{23} $$

In region II between h_{S1} and h_{S2}, the scaling α_2 is used to scale with decay separation between region II and region I, as the decaying effect won't be stopped counted for until leaving height h_1.

$$ \frac{C_{II}}{4\pi a_{h1}^2(h_{S2} - h_1)} = \frac{1}{4\pi a_{h1}^2(h_{S2} - h_1)} \cdot \alpha_2 \cdot {}_{C}N(h_{S1}, h_{S2}) \cdot N_0 \left[\tau(h_1, h_{S1}) + \tau(h_{S1}, h_{S2})\right]. \tag{24} $$

Notice the critical number comes from the single shell condition of region II as ${}_{\mathrm{C}}\mathrm{N}(\mathrm{h_{S1}},\mathrm{h_{S2}})$. However, the decaying effect in the multi-shell requires the decay to go through both region II and region I, that is the a total decay requires to go through $\mathrm{h_{S2}}$, and $\mathrm{h_{S2}}$, and then $\mathrm{h_{S1}}$ and $\mathrm{h_1}$. In region III between $\mathrm{h_{S2}}$ and $\mathrm{h_{S3}}$, similar to region II, α_3 is used to scale the critical number from single-shell derivation,

$$\frac{\mathrm{C_{III}}}{4\pi \mathrm{a}_{\mathrm{h1}}^2(\mathrm{h_{S3}}-\mathrm{h_1})} = \frac{1}{4\pi \mathrm{a}_{\mathrm{h1}}^2(\mathrm{h_{S3}}-\mathrm{h_1})} \cdot \alpha_3 \cdot {}_{\mathrm{C}}\mathrm{N}(\mathrm{h_S},\mathrm{h_{S2}}) \cdot \mathrm{N_0}\left[\tau(\mathrm{h_1},\mathrm{h_{S1}}) + \tau(\mathrm{h_{S1}},\mathrm{h_{S2}} + \tau(\mathrm{h_{S2}},\mathrm{h_{S3}})\right]. \tag{25}$$

Consider the three expressions Eqs. 23-25 for regions I, II, III and the shelling-independent constant Eq. 20, the equations need to satisfy the following condition at the runaway condition,

$$\frac{\mathrm{C_I}}{4\pi \mathrm{a}_{\mathrm{h1}}^2(\mathrm{h_{S1}}-\mathrm{h_1})} + \frac{\mathrm{C_{II}}}{4\pi \mathrm{a}_{\mathrm{h1}}^2(\mathrm{h_{S2}}-\mathrm{h_1})} + \frac{\mathrm{C_{III}}}{4\pi \mathrm{a}_{\mathrm{h1}}^2(\mathrm{h_{S3}}-\mathrm{h_1})} = \frac{1}{\sigma_{\mathrm{f}}\mathrm{V}}. \tag{26}$$

This Eq. 26 means whether the multi-shell formulation is considered or a single-shell between $\mathrm{h_1}$ and $\mathrm{h_{S3}}$ is used, the collision nature throughout the region should be conserved. The conservation should be limited by the shelling-independent constant introduced in Eq. 20 and Eq. 21.

After some manipulation, the constrain for multi-shell condition is expressed as Eq. 27. This equation expresses a constrain the single-shell critical numbers need to satisfy when considering the coexisting multi-shell condition.

$$\boxed{\begin{aligned} &\alpha_1 + \alpha_2\left[\frac{(\mathrm{h_{S1}}-\mathrm{h_1})}{(\mathrm{h_{S2}}-\mathrm{h_1})} \cdot \frac{\mathrm{a}_{\mathrm{h_{S1}}}^3 \cdot \mathrm{V_0}(\mathrm{h_{S1}})\,\rho_{\mathrm{a}}(\mathrm{h_{S1}})}{\mathrm{a}_{\mathrm{h_1}}^3 \cdot \mathrm{V_0}(\mathrm{h_1})\,\rho_{\mathrm{a}}(\mathrm{h_1})} + \frac{(\mathrm{h_{S2}}-\mathrm{h_{S1}})}{(\mathrm{h_{S2}}-\mathrm{h_1})} \cdot \frac{\mathrm{a}_{\mathrm{h_{S1}}}^2}{\mathrm{a}_{\mathrm{h_1}}^2}\right] + \\ &\alpha_3\left[\frac{(\mathrm{h_{S1}}-\mathrm{h_1})}{(\mathrm{h_{S3}}-\mathrm{h_1})} \cdot \frac{\mathrm{a}_{\mathrm{h_{S2}}}^3 \mathrm{V_0}(\mathrm{h_{S2}})\,\rho_{\mathrm{a}}(\mathrm{h_{S2}})}{\mathrm{a}_{\mathrm{h1}}^3 \mathrm{V_0}(\mathrm{h_1})\,\rho_{\mathrm{a}}(\mathrm{h_1})} + \frac{(\mathrm{h_{S2}}-\mathrm{h_{S1}})}{(\mathrm{h_{S3}}-\mathrm{h_1})} \frac{\mathrm{a}_{\mathrm{h_{S2}}}^3 \mathrm{V_0}(\mathrm{h_{S1}})\,\mathrm{a_a}(\mathrm{h_{S2}})}{\mathrm{a}_{\mathrm{h_{S1}}}\mathrm{a}_{\mathrm{h_1}}^2 \mathrm{V_0}(\mathrm{h_{S1}})\,\rho_{\mathrm{a}}(\mathrm{h_{S1}})} + \frac{\mathrm{h_{S3}}-\mathrm{h_{S2}}}{\mathrm{h_{S3}}-\mathrm{h_1}} \cdot \frac{\mathrm{a}_{\mathrm{h_{S2}}}^2}{\mathrm{a}_{\mathrm{h_1}}^2}\right] = 1 \end{aligned}} \tag{27}$$

Generalizing into n shells We generalize the 3-shell condition to the n-shell case as follows.

First, define $h_{s_0} \equiv h_1$, and for $m \geq 1$ introduce the cumulative interior multiplier

$$\Gamma_{\mathrm{m}} \stackrel{\mathrm{def}}{=} \frac{\mathrm{a}_{\mathrm{h_{Sm}}}^3 \mathrm{V_0}(\mathrm{h_{Sm}})\,\rho_{\mathrm{a}}(\mathrm{h_{Sm}})}{\mathrm{a}_{\mathrm{h_{S(m-1)}}}\mathrm{a}_{\mathrm{h_1}}^2 \mathrm{V_0}(\mathrm{h_1})\,\rho_{\mathrm{a}}(\mathrm{h_1})}, \qquad \Gamma_0 \equiv 1. \tag{28}$$

Next, define the segment weights

$$\mathrm{W_{k,j}} \stackrel{\mathrm{def}}{=} \frac{\mathrm{h_{Sj}} - \mathrm{h_{S(j-1)}}}{\mathrm{h_{S_k}} - \mathrm{h_1}}, \qquad 1 \leq \mathrm{j} \leq k,\ k \geq 1, \tag{29}$$

and "area" ratio

$$\mathscr{A}_{\mathrm{m}} \stackrel{\mathrm{def}}{=} \frac{\mathrm{a}_{\mathrm{h_{Sm}}}^2}{\mathrm{a}_{\mathrm{h_1}}^2}. \tag{30}$$

With these definitions, the n–shell condition reads elegantly as

$$\boxed{\alpha_1 + \sum_{k=2}^{n} \alpha_k \left[\sum_{\mathrm{j}=1}^{k-1} \mathrm{W}_{k,\mathrm{j}}\Gamma_j \;+\; \mathrm{W}_{k,k}\,\mathscr{A}_{k-1}\right] = 1.} \tag{31}$$

Substituting $n = 3$ reproduces the structure of the original 3-shell expression in Eq. 27.

2.4 Scaling in 3-shell Formulation

The scaling factor α_k converts the single-shell critical number in Eq. 17 into the generalized multi-shell condition given in Eq. 31. The explicit three-shell condition is shown in Eq. 27. To illustrate the role of scaling, we investigate several representative cases for the three-shell configuration. The three cases, differing in shell separation, are:

- **Case 1:** $h_1 = 200$ km, $h_{S1} = 600$ km, $h_{S2} = 650$ km, $h_{S3} = 700$ km;
- **Case 2:** $h_1 = 200$ km, $h_{S1} = 250$ km, $h_{S2} = 300$ km, $h_{S3} = 350$ km;
- **Case 3:** $h_1 = 200$ km, $h_{S1} = 250$ km, $h_{S2} = 300$ km, $h_{S3} = 400$ km.

These examples highlight different approaches to shelling in the design of the space system. Case 1 assumes equal spacing between the higher shells, while lower altitudes are treated as more manageable and thus grouped into a single, widely separated shell. Case 2 represents the widely adopted approach of dividing the orbital region into shells of equal width. Case 3 reflects a scenario in which the upper shells are expected to be less crowded, allowing for a larger shelling width at higher altitudes.

By requiring α_3 to remain physically meaningful, i.e., non-negative, the Pareto fronts for the scaling factors α_1, α_2, α_3 are shown in the left panels of Fig. 2. The right panels illustrate the feasible region for α_3 as a colormap, with contours marking the boundaries of the coexisting multi-shell condition, and the limiting cases indicated by the red line and its intersections with the coordinate axes. The color scale for α_3 represents the maximum allowable scaling for shell 3 when the number of intact objects in the other shells is zero; the same interpretation applies to the intersections of the limit line with the axes.

In Case 1 (top panel), the maximum scaling for α_3 reaches nearly 8. This arises because the third shell, defined between 650 km and 700 km, is comparatively thin. When contrasted with the much larger lower shells, this configuration leads to a higher expected scaling relative to the single-shell condition. In practice, lower shells can typically host more satellites, since stronger atmospheric drag at those altitudes shortens the orbital lifetime and thereby reduces the probability of generating long-lived breakup debris [1]. However, when the intact objects are restricted to specific shells, the otherwise unused volume between the thin upper shell and the decay region is effectively "reused," increasing the upper bound on the allowable population in that shell.

We further investigate the extension of Case 2 and Case 3. Different width for the higher shell is used to find the sets of Pareto Front, shown in Fig. 3, satisfying three-shell condition Eq. 27, an example of the multi-shell condition Eq. 31.

We observe that as the width of the highest shell increases, the maximum scaling approaches unity, corresponding to the single-shell condition. This behavior is consistent with the expectation that treating the entire region as one large shell, with two sufficiently small lower shells, should recover the single-shell formulation.

2.5 Multi-Shell Trade Study

The scaling factors that transform the single-shell critical condition into the multi-shell framework provide a theoretical framework to investigate scenarios in which the number of intact objects is redistributed across different orbital shells. In practice, orbital preferences and operational demands do not necessarily yield an even distribution of objects, and the natural evolution of orbital populations requires a framework capable of evaluating these uneven combinations.

To illustrate this, we consider the simplified case of three shells. We first apply the critical number formulation in Eq. 17 to determine the critical numbers under the single-shell condition, as previously examined in [1, 4, 5]. D'Ambrosio and Linares [1], building on Kessler's earlier work [3–5] and using the NASA Standard Breakup Model (SBM), derived from the P-78 dataset, reported an average of 497 fragments per breakup. The shell boundaries and corresponding single-shell critical numbers for the three-shell configuration are summarized in Table 1.

Altitudes (km)				Single-Shell Critical Numbers		
h_1	h_{S1}	h_{S2}	h_{S3}	${}_R N_{i,\hat{V}1}\,(h_1, h_{S1})$	${}_R N_{i,\hat{V}2}\,(h_{S1}, h_{S2})$	${}_R N_{i,\hat{V}3}\,(h_{S2}, h_{S3})$
200	600	650	700	2.969277×10^4	1.313683×10^4	5.811331×10^3

Table 1: Shell boundaries and corresponding single-shell critical numbers.

Using these critical numbers, we compute the Pareto fronts for the three-shell configuration. Figure 4 illustrates the feasible regions (green) for runaway scenarios, along with contour lines corresponding to the total number of intact objects. These contours provide insight into how redistributing objects across shells affects the overall stability of the environment.

The three-dimensional surface in Fig. 4 captures all possible runaway scenarios arising from different combinations of intact objects across the three shells. As a result, the critical number for the entire orbital environment is not a

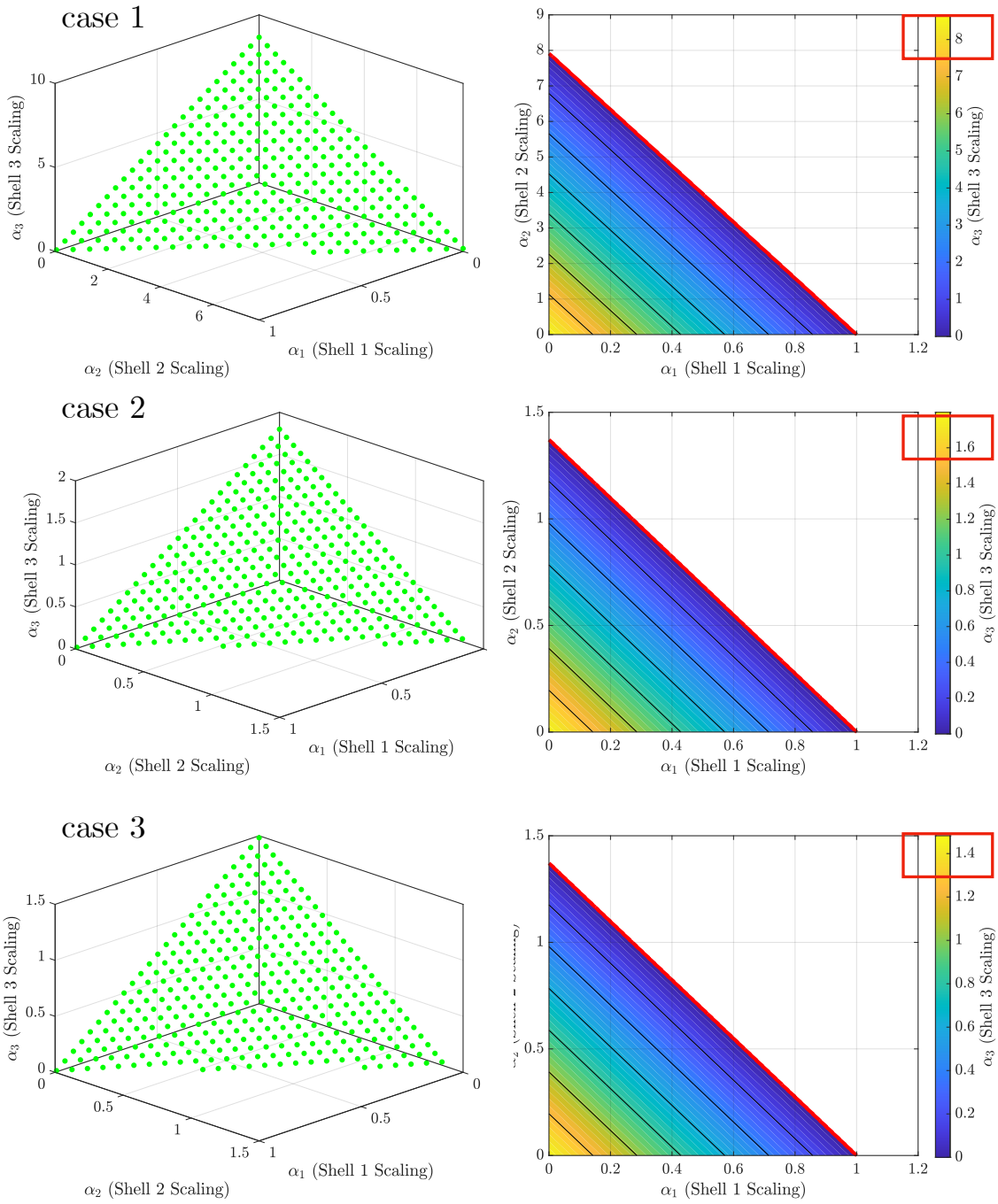

Fig. 2: Multi-shell conditions scaling from single-shell conditions. Left panels are the Pareto Front. Right panels are the contour and colormap for scaling α_3. Notice the circled red parts illustrate the different maximum number for scaling α_3.

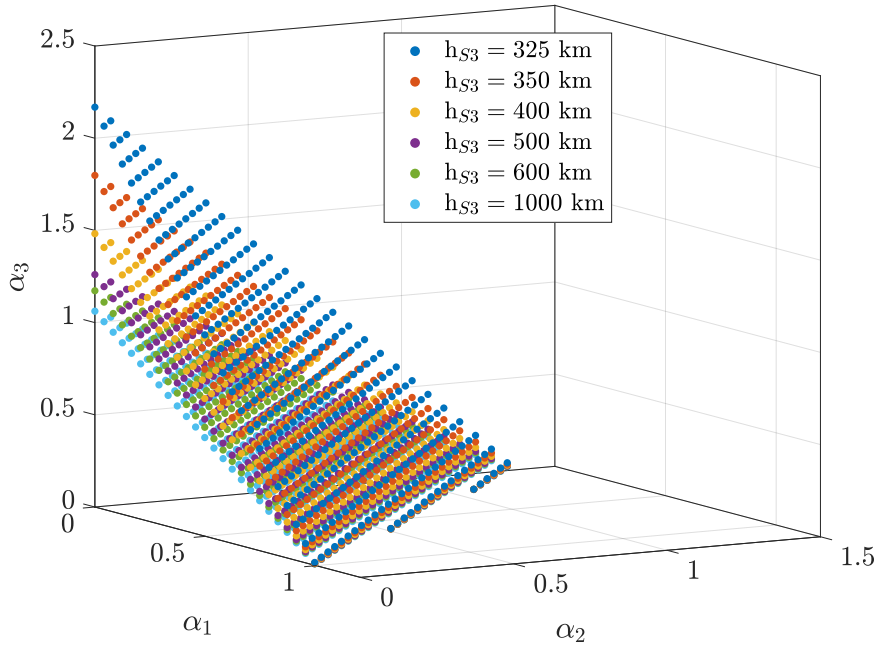

Fig. 3: Pareto Fronts from differing shell widths for the highest shell in three-shell condition.

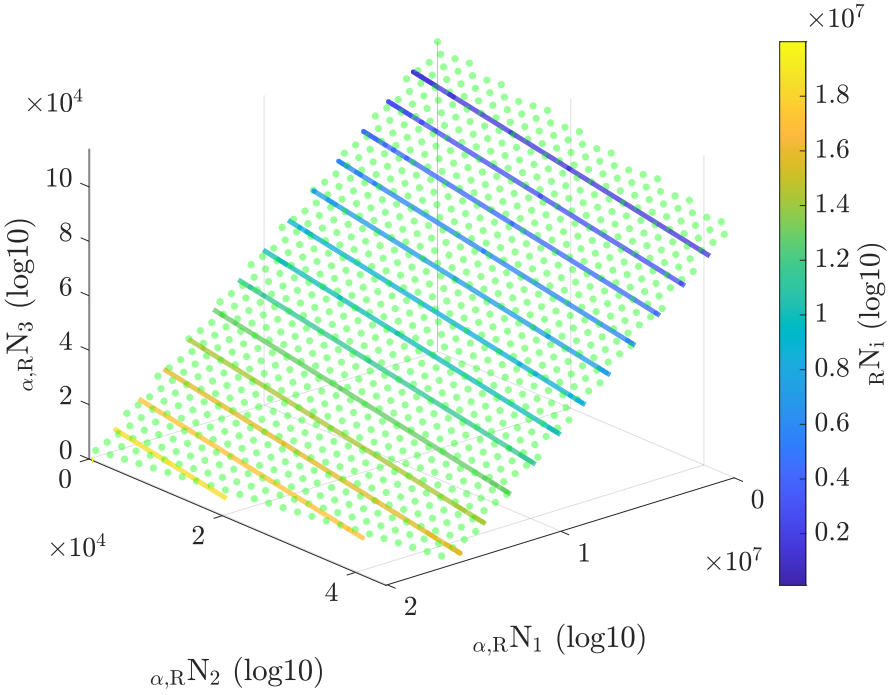

Fig. 4: Pareto fronts of the critical numbers for the three-shell configuration (Table 1). Green regions indicate feasible conditions, consistent with Fig. 2. Contour lines correspond to the total number of intact objects.

single value but rather follows a distribution. This distribution is shown in Fig. 5, where the number of intact objects is presented on a $\log_{10}$ scale.

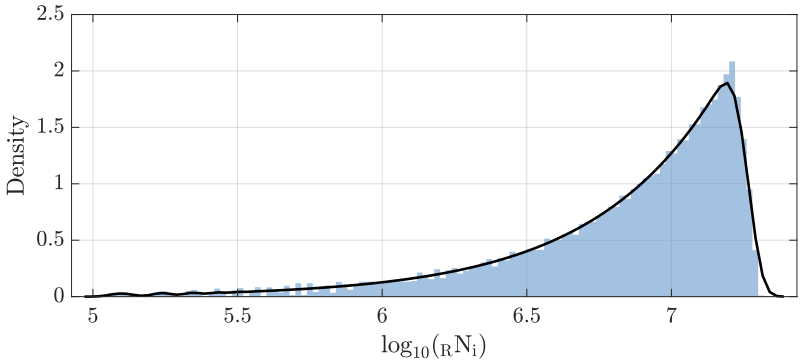

Fig. 5: Distribution of the critical number of intact objects at runaway scenario for Case 1 (Table 1). The number of intact objects is shown on a $\log_{10}$ scale.

3. CONCLUSION

We derived a multi-shell space safety condition, extending Kessler's classical single-shell critical number and critical density formulation. By revisiting Kessler's original derivation, we clarified both the shelling-dependent nature of the formulation and its underlying single-shell assumption. From this analysis, we identified a shelling-independent constant that depends only on the intrinsic nature of collisions.

Building on this result, we introduced the concept of the fragmentation footprint, defined as the accumulation of breakup fragments from generation to total decay per breakup for each intact object. By combining the fragmentation footprint with the shelling-independent constant, we established a physical constraint that governs the general multi-shell condition. We then explicitly derived both the three-shell formulation that satisfies this condition, as well as its generalized *n*-shell extension.

In the numerical analysis, we focused in detail on the three-shell formulation. Pareto fronts under different cases were examined to illustrate the effect of the constraint, and we investigated the influence of shelling width. Notably, when the shelling width becomes sufficiently large, the scaling factor for that shell approaches unity, thereby recovering the single-shell condition. This result provides a direct verification of our derivation.

Moving to the implications, by explicitly computing critical numbers for a three-shell case based on the single-shell formulation, we constructed—for the first time—a surface representing the full set of possible outcomes in the multi-shell condition. Our results show that the resulting critical number is no longer a single value, but instead spans a distribution, reflecting the richer dynamics of the multi-shell environment.

[1] Andrea D'Ambrosio and Richard Linares. Carrying capacity of low earth orbit computed using source-sink models. *Journal of Spacecraft and Rockets*, 61(6):1447–1463, November 2024.

[2] Daniel Jang, Davide Gusmini, Peng Mun Siew, Andrea D'Ambrosio, Simone Servadio, Pablo Machuca, and Richard Linares. A new monte-carlo model for the space environment, 2024.

[3] Donald J. Kessler. Collision probability at low altitudes resulting from elliptical orbits. *Advances in Space Research*, 10(3-4):393–396, January 1990.

[4] Donald J. Kessler. Critical density of spacecraft in low earth orbit: Using fragmentation data to evaluate the stability of the orbital debris environment. Technical Report LMSEAT-33303, Lockheed Martin Space Operations Company, 2400 NASA Rd 1, Houston, TX 77058, February 2000.

[5] Donald J. Kessler and Phillip D. Anz-Meador. Critical number of spacecraft in low Earth orbit: using satellite fragmentation data to evaluate the stability of the orbital debris environment. In Huguette Sawaya-Lacoste, editor, *Space Debris*, volume 1 of *ESA Special Publication*, pages 265–272, October 2001.

[6] Giovanni Lavezzi, Daniel Jang, and Richard Linares. Stable and sustainable orbital capacity solutions in low earth orbit. *Acta Astronautica*, 235:736–746, October 2025.

[7] Minoo Rathnasabapathy, Francesca Letizia, Stijn Lemmens, Moriba Jah, Simon Potter, Nikolai Khlystov, Kristi Acuff, Miles Lifson, Scott Dorrington, Sina Es haghi, Emmanuelle David, Jean-Paul Kneib, and Danielle Wood. Space sustainability rating: Designing a composite indicator to incentivize satellite operators to pursue long-term sustainability of the space environment. *Acta Astronautica*, 232:622–632, July 2025.